Journal of
*Marine Science and Engineering*

MDPI

*Article*

# A Low-Cost Communication-Based Autonomous Underwater Vehicle Positioning System

**Raphaël Garin [1], Pierre-Jean Bouvet [1,*], Beatrice Tomasi [1,2], Philippe Forjonel [1] and Charles Vanwynsberghe [1,3]**

[1] LabISEN, ISEN Ouest, 29200 Brest, France; beto@norceresearch.no (B.T.); philippe.forjonel@isen-ouest.yncrea.fr (P.F.); charles.vanwynsberghe@tii.ae (C.V.)
[2] Norwegian Research Centre, 5008 Bergen, Norway
[3] Technology Innovation Institute, Masdar City, Abu Dhabi 9639, United Arab Emirates
* Correspondence: pierre-jean.bouvet@isen-ouest.yncrea.fr

**Abstract:** Underwater unmanned vehicles are complementary with human presence and manned vehicles for deeper and more complex environments. An autonomous underwater vechicle (AUV) has automation and long-range capacity compared to a cable-guided remotely operated vehicle (ROV). Navigation of AUVs is challenging due to the high absorption of radio-frequency signals underwater and the absence of a global navigation satellite system (GNSS). As a result, most navigation algorithms rely on inertial and acoustic signals; precise localization is then costly in addition to being independent from acoustic data communication. The purpose of this paper is to propose and analyze the performance of a novel low-cost simultaneous communication and localization algorithm. The considered scenario consists of an AUV that acoustically sends sensor or status data to a single fixed beacon. By estimating the Doppler shift and the range from this data exchange, the algorithm can provide a location estimate of the AUV. Using a robust state estimator, we analyze the algorithm over a survey path used for AUV mission planning both in numerical simulations and at-sea experiments.

**Keywords:** underwater navigation; Kalman filter; particle filter; underwater acoustic communications; Doppler shift estimation; autonomous underwater vehicle; integrated sensing and communication



**Citation:** Garin, R.; Bouvet, P.-J.; Tomasi, B.; Forjonel, P.; Vanwynsberghe, C. A Low-Cost Communication-Based Autonomous Underwater Vehicle Positioning System. *J. Mar. Sci. Eng.* **2024**, *12*, 1964. https://doi.org/10.3390/jmse12111964

Academic Editors: Xiao Liang, Rubo Zhang and Xingru Qu

Received: 5 September 2024
Revised: 14 October 2024
Accepted: 17 October 2024
Published: 1 November 2024



## 1. Introduction

Unmanned underwater missions can be performed by either ROVs or AUVs. Both of them integrate payloads and the mission's specific tool set, such as gripper jaws [1] or sonar detection. For the first drone category, the link between the operator and the ROV is an umbilical cable. Its length depends on the mission area, typically covering 300 m at the surface and reaching depths of up to 100 m for small ROVs. Navigation and telemetry are made through this cable, and ROVs usually have a camera. ROVs have many advantages, such as their price, handling, and live telemetry. Underwater ROVs can be used for video streaming of corals or shipwrecks for inspection, remote actuation, or real-time measurements.

In the second category of unmanned underwater vehicles, AUVs, cable communication is replaced by wireless communication, allowing the robot to extend its mission coverage as well as its movement capabilities, the only remaining constraint being the maximal battery autonomy. Compared to an ROV, an AUV can go deeper and operate in a larger radius with a given trajectory with no manual guidance except from mission planning. Usual applications are underwater surveillance, inspection, exploration, or mapping within both civil and military fields [2].

Yet, AUVs face many challenges. The underwater channel absorbs radio frequency (RF) waves after a few meters and optical waves after some tens of meters [3]. As a result, underwater acoustic (UWA) communications are privileged for long-range scenarios.

Underwater sound propagation speed is relatively low (around 1500 m/s) compared to RF or optical waves in the air (similar to light speed around $3 \times 10^8$ m/s). Low propagation speed yields an important Doppler shift, and UWA propagation is characterized by strong multipath echoes induced by boundary (i.e., sea bottom and surface) reflections. Both Doppler drift and multipath echoes need to be compensated for by the receiving system [4–6]. Moreover, in order to follow an intended trajectory, the AUV requires to know its position in real time. However, as stated before, since RF signals are absorbed by water after a few meters of depth, the GNSS localization system is not available underwater. As a result, AUV positioning and navigation are active research topics [2,7].

Despite recent research progress and industrial products, current localization and navigation technologies share two main flaws. The first consists of the use of costly inertial sensors or of an infrastructure of several acoustic beacon nodes deployed in very accurate positions to achieve the needed accuracy throughout the AUV mission. The second limitation is the lack of integration between positioning and communication systems. Even if both systems are based on acoustic waves, positioning systems used for localization use some navigation-specific transmissions that are often not suitable for data exchanges [8]. Note that in current 6G research, integrated sensing and communication is a hot topic, driving the development of theory and future standards to simultaneously provide communication and user positioning capabilities [9].

This paper proposes an algorithm where a single fixed beacon simultaneously communicates with an AUV while positioning it. In this lightweight infrastructure scenario (with only one beacon instead of four), the vehicle regularly receives data from the transmitting beacon. By assuming that these two parts are synchronized in time, range estimation between them is possible by computing the time of flight (TOF) of the transmitted signal. Moreover, the receiver has to estimate the Doppler scaling factor induced by the relative speed between the AUV and the beacon. This Doppler shift estimate will have to be compensated for when decoding the data [6]. The Doppler shift estimate is also a representation of the vehicle-beacon relative velocity. Combining the relative velocity, the bearing angle of the AUV, its heading angle, and the range to the beacon, we can compute the velocity of the vehicle projected along the linear trajectory connecting the vehicle and the beacon. While the bearing angle is estimated, the heading angle is measured by an inertial sensor such as an inertial measurement unit (IMU) that is modeled in this paper by including measurement noises and biases typical of a micro-electromechanical system (MEMS) IMU. All this information is filtered within a state estimator. Many estimators exist in the literature [10]; in this paper, we choose the extended Kalman filter (EKF). The main objective of this paper is to model and simulate this low-cost underwater localization approach and then demonstrate its feasibility in a real-world scenario.

The rest of the paper is organized as follows: we first review the state-of-the-art and previous work in Section 2. The details of our model and algorithm are provided in Section 3. In Section 4, we present the localization performance evaluation obtained in numerical simulations, by varying several system parameters and noises, and in at-sea experiments. Finally, in Section 5, a conclusion is drawn by summarizing the advantages and limitations of the proposed algorithm.

## 2. Existing Methodologies

### *2.1. Multiple-Transponder Systems*

If the desired accuracy error scales at the centimeter level, multiple acoustic transponder systems are required. Combined with a powerful inertial navigation system (INS) (typically fiber optical gyroscope (FOG) technology) and Doppler velocity log (DVL) sensors, the AUV localization is precise, with a positioning error below 1% at the end of the mission. Acoustic localization/navigation techniques fall into two categories [2]:

1. Long baseline (LBL) and GPS intelligent buoy (GIB): One of the first UWA localization techniques developed in the middle of the 1970s by [11]. The long baseline (LBL) procedure consists of a set of UWA transponders precisely disposed of on the seabed

around the mission area. Each transponder has a known precise position and is synchronized with the others. Therefore, in addition to beacon deployment, the calibration of their relative position and timing becomes a key step. The AUV position is then estimated through triangulation with respect to its range to all transponders. Ranges are computed with TOF or time difference of arrival (TDOA) techniques. At least three transponders are recommended to have good accuracy. The GPS intelligent buoy (GIB) method is similar to LBL. The difference is that transponders are installed on surface buoys and not on the seafloor. This reduces calibration costs.

2. Short baseline (SBL): Beacons are deployed at opposite sides of a surface vessel (or platform). TDOA triangulation is then used to determine the AUV position. The baseline length is designed in relationship with the vessel size. The main limitation of short baseline (SBL) is its localization accuracy.

These techniques can be hybrid, such as sparse LBL. It is common to use data fusion algorithms between acoustic transponder positioning and dead-reckoning positioning systems. In that way, the inaccuracies of one technique can be compensated for by the better performance of the other one and vice versa. For instance, LBL positioning could be used without any dead-reckoning measurements, but its performance will be less precise due to the sensor's noises or the varying acoustic physical variables of the environment. Dead-reckoning (inertial navigation) can be implemented without any acoustic transponder, but the position estimates will have a considerable drift over time. For a small AUV, the currently available solution can have the following disadvantages: computational complexity, costs, infrastructures (LBL, SBL...), precise calibration (FOG INS), and heavy and costly DVL sensors. These solutions are better suited for offshore industry or bathymetric applications where precision is crucial.

### 2.2. Single-Transponder Systems

For systems using a single beacon at a known position, it is common to use ultra-short baseline (USBL) [7] or range-only single beacon (ROSB), as the methods proposed in [10,12,13]. These methods are easier to deploy for low-cost missions than those described in Section 2.1. The USBL system estimates the AUV's position using multiple transmissions done by the UWA communication system feeding an EKF with TDOA and bearing angles. Depending on the user's choice, it is possible to only carry out live tracking of the drone rather than helping the drone to reposition itself. The architecture of the anchor is more sophisticated than a simple underwater transceiver. More than three receiving hydrophones are needed to compute the bearing angle estimation. But, it is common to use four receivers at a short distance to optimize this estimation (usually below 10 cm). Kongsberg, EXail, Blueprint, and Sonardyne propose these systems [14]. Range-based navigation (ROSB) is the fastest to implement and the cheapest. Using a series of TOF or TDOA measurements, the only estimation made is the range between the fixed beacon at a known position and the moving AUV. This solution and USBL require information about sound speed and depth. USBL also requires either a differential global positioning system (DGPS) and/or an attitude and heading reference system (AHRS) in order to position the bearing angle in relation to the north. The physical implementation thus requires physical stability in rotation, whereas ROSB is rotationally independent.

One can also cite research subjects such as virtual LBL [15]. The main idea is to add virtual transponders with range measurements and predicted dead-reckoning positions. But, dead-reckoning navigation precision is greatly affected by the presence of a high-cost DVL sensor.

Lastly, industrial products from companies such as Exail and Sonardyne developed sparse LBL [16]. This is a positioning system that uses a single transponder. Range measurements from acoustics are coupled with a mandatory INS (or INS/DVL) to enhance AUV positioning. It has the advantage of being usable with more transponders according to the desired accuracy. It consists of a series of acoustical pings.

It is important to note that it is possible to use dead-reckoning/inertial navigation INS without any acoustic system. It can be implemented through three technologies: MEMS for the cheapest and smallest solution, FOG for strong stability over time, and ring laser gyroscope (RLG) as the historically strong stability solution, but its space requirement is not suitable for a micro-AUVs. Depending on the sensor performance, the drift bias makes the positioning error grow even more. This is usually called the bias instability. The instability range is from 0.01°/h for the high-end FOG to 2°/h for the cheapest FOG. As for MEMS technology, the range is from 2°/h for high-end systems to 10°/h for the smallest systems (such as smartphones, for example). The DVL can reduce this error, but its technology range is limited by the depth level of the AUV. A DVL works by emitting acoustic pulses downward and measuring the frequency shift of the returned signals reflected from the seabed or particles in the water. This frequency shift, caused by the Doppler effect, is used to calculate the vehicle's velocity relative to the bottom or water column. Equipped with multiple beams and an IMU, a DVL can determine not only the speed in three dimensions but also the heading and pitch, making it essential for precise navigation of underwater vehicles like ROVs and AUVs. Depending on the DVL, the distance between the seafloor and AUV must be 300 m to 6000 m at most for the smallest ones.

As shown previously, ROSB is a good solution to perform simultaneous navigation and communication with a minimum number of sensors. However, such a system provides large localization errors [10] and is demonstrated to be current dependent without a DVL [13]. In practice, the ROSB method needs to be combined with an acoustic Doppler current profiler (ADCP) or DVL to achieve good accuracy. The idea of combining range and Doppler-shift measurements to perform underwater target tracking was first introduced by Diamant et al. in [17]. However, the authors used several anchor nodes to provide the TOF, bearing angle, and Doppler information. In [18], the authors proposed a ROSB method combined with Doppler shift measurements as a navigation algorithm for an AUV performing a lemniscate trajectory. Simulation results were promising: for communication made every 10 s, the positioning accuracy error was contained below 10 m for a 6000 $m^2$ mission area. Later on [19], the authors conducted an experiment using the same trajectory in a 3 $m^2$ pool. Despite numerous reflections, sensor noises, and a small induced Doppler shift, the algorithm kept a low positioning error. Finally, the algorithm was evaluated during at-sea experiments in [20].

In the current paper, we extend the work in [20] by conducting extensive simulations with realistic estimation noises and biases. The impact of time between successive communications on the positioning accuracy is also analyzed. Performance comparison against the conventional ROSB method is carried out. Finally, numerical simulation results are compared against experimental results.

## 3. Materials and Methods

### *3.1. Problem Formulation*

We focus on a two-dimensional problem by omitting the depth axis. In fact, it is straightforward to implement the last axis by adding a low-cost pressure sensor. The accuracy of this sensor category is in centimeters and is easily implementable in a small AUV.

We consider a mission where an AUV performs a survey path (as typically used in side scan sonar missions) and is equipped with an IMU, a global positioning system (GPS), and an acoustic modem. While navigating, the AUV receives acoustic data from a fixed surface beacon with a submerged transponder. The chosen trajectory for the mission is a classical boustrophedon trajectory, also called a survey path, and has a mission duration named $T_{\text{mission}}$. The reference beacon position is denoted as $\begin{pmatrix} x_{\text{ref}} & y_{\text{ref}} \end{pmatrix}^T$, and is obtained in practice with a GNSS receiver that provides typically metric accuracy. To enhance this value, a DGPS system can be mounted to the station. DGPS works with two spaced GNSS receivers. Compared to one GNSS antenna system, it also provides a precise azimuth angle. To obtain centimetric accuracy, it is possible to add a RTK (real-time kinematic) antenna to

the DGPS system.

Table 1 summarizes the sensor's public price available. As the AHRS is a critical component, this sensor should not be subject to a cost-reduction target. Propeller parts and embedded electronics are not taken into account here. The costly component of the proposed system is the UWA modem. Furthermore, there is no ultra-low-cost mass-market solution (below EUR 2000). The final solution embedded into a micro-AUV offers real-time communication between surfaces while positioning the AUV. Using the less expensive mass-market UWA modem, the proposed navigation algorithm cost is below EUR 4000, which gives the proposed system a relatively low-cost label compared to conventional positioning systems based on USBL or DVL.

**Table 1.** Navigation algorithm sensors standard price.

| Sensor | Standard Public Price | Measurement(s) |
|---|---|---|
| AHRS | EUR 1200 | Euler angles |
| Pressure | EUR 90 | Depth and temperature |
| GPS | EUR 20 | Surface position |
| UWA modem | from EUR 500 [21] to 2500 € [22] | Communication, Doppler, and range |

The proposed positioning algorithm is depicted in Figure 1. Parameters and noise initialization correspond to the initialization of mission parameters and filter input parameters (observation and state functions, covariance matrices, and command). The command update refers to the linearization feedback method leading to command vector **u** described in Section 3.2. If no acoustic communication frame is available, the measurements rely only on IMU data (dead reckoning); if yes, acoustic communication decoding brings additional measurements (distance and relative speed), as described in Section 3.5. The time between two received communication frames is denoted as $T_{\text{com}}$. Measurements are then fed to the filter estimator (see Section 3.6).

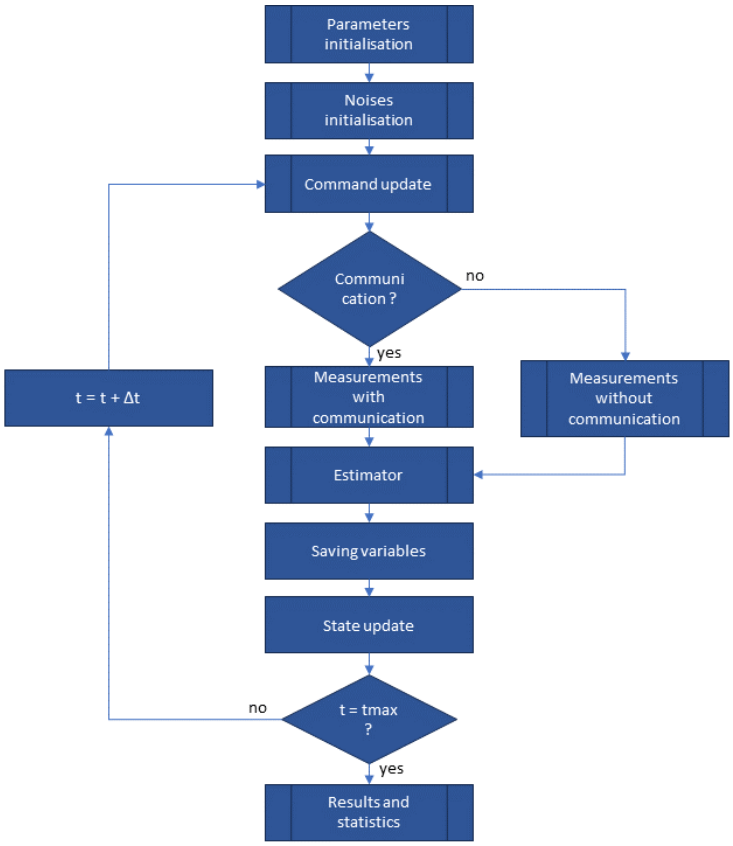


**Figure 1.** Positioning algorithm.

### *3.2. Drone Scheduling*

The dynamic of the AUV in a 2D plan is depicted in Figure 2. We define the ground truth vector $\mathbf{X} = \begin{pmatrix} x & y & \psi & v \end{pmatrix}^T$ with $\begin{pmatrix} x & y \end{pmatrix}^T$ as the actual position of the drone; $\psi$ is the heading angle of the drone, and $v$ is its speed. We note $\omega_b$ as the bearing angle between the drone and the beacon, and $v_r$ is the relative speed of the drone projected in the direction of the reference beacon. The 2D trajectory is defined by $\begin{pmatrix} x_d & y_d \end{pmatrix}^T$ with $x_d$ and $y_d$, respectively, and the $x$-axis and the $y$-axis coordinates of a point on the trajectory at sampling time $t$.

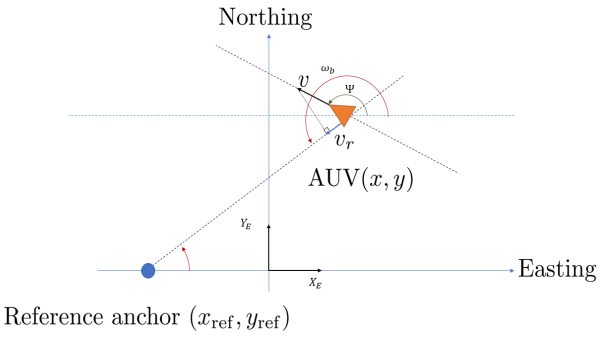


**Figure 2.** Dynamic of the AUV.

We assume that the drone command is made through the **u** vector:

$$\mathbf{u} = \begin{pmatrix} \Omega \\ a \end{pmatrix} = \begin{pmatrix} \dot{\psi} \\ \dot{v} \end{pmatrix}, \tag{1}$$

where $\Omega$ is the rotational speed of the AUV, and $a$ is its acceleration.

Using the linearization feedback method, the drone command vector can be expressed as follows:

$$\begin{pmatrix} \Omega \\ a \end{pmatrix} = \begin{pmatrix} -v \cdot \sin(\psi) & \cos(\psi) \\ v \cdot \cos(\psi) & \sin(\psi) \end{pmatrix}^{-1} \begin{pmatrix} (x_d - x) + 2(\dot{x}_d - v \cdot \cos(\psi)) + \ddot{x}_d \\ (y_d - y) + 2(\dot{y}_d - v \cdot \sin(\psi)) + \ddot{y}_d \end{pmatrix}. \tag{2}$$

The model is updated at each time $\Delta t$ by the following equation :

$$\mathbf{X}(t) = \mathbf{X}(t - \Delta t) + f_t(\mathbf{X}, \mathbf{u}) \cdot \Delta t, \tag{3}$$

with

$$f_t(\mathbf{X}, \mathbf{u}) = \begin{pmatrix} v\cos(\psi) \\ v\sin(\psi) \\ \Omega \\ a \end{pmatrix} = \dot{\mathbf{X}}. \tag{4}$$

In practice, the open-source software "ArduPilot" [23] can carry out the planning part of the drone (trajectory/linearization/control) alone from way-points given by positioning estimation.

### 3.3. AUV Model

The use of Kalman filtering for motion estimation requires a discrete time representation of the state space of the drone behavioral model. For the model, we define the following state equations:

$$\begin{cases} \mathbf{z}_{k+1} = f(\mathbf{z}_k, \mathbf{u}_k) + \mathbf{w}_k \\ \mathbf{y}_k = g(\mathbf{z}_k) + \mathbf{v}_k \end{cases}, \tag{5}$$

where $\mathbf{z}_k$ is the state vector of the AUV at sampling time $k$, $\mathbf{u}_k$ is the command vector $\mathbf{u}$ at sampling time $k$, $f(\mathbf{z}_k, \mathbf{u}_k)$ is the state equation, $g(\mathbf{z}_k)$ is the observation function, and finally, $\mathbf{w}_k$ and $\mathbf{v}$ are, respectively, the state and observation noises. The state vector of the AUV is defined as follows:

$$\mathbf{z} = \begin{pmatrix} x & y & \psi & v & \Omega & a \end{pmatrix}^T. \tag{6}$$

The state equation becomes the following:

$$\mathbf{f}(\mathbf{z}, \mathbf{u}) = \begin{pmatrix} x + v\,\Delta_t \cos\psi \\ y + v\,\Delta_t \sin\psi \\ \psi + \Delta_t \Omega \\ v + \Delta_t a \\ \Omega \\ a \end{pmatrix}. \tag{7}$$

### 3.4. Underwater Acoustic Communication System

We assume that the beacon and the AUV regularly exchange data with each other using underwater acoustic communications. At each time interval $T_{\text{com}}$, the beacon transmits the acoustic frame depicted in Figure 3, which is received by the AUV. On the one hand, the acoustic frame includes a main signal centered on $f_0$ with bandwidth $B$ carrying $N_p$ pilot symbols (for synchronization and channel estimation) and $N_d$ useful data symbols. On the other hand a pure-tone signal with frequency $f_{pt}$ is used for Doppler shift estimation. The frame starts and ends with $N_d$ null symbols to avoid interference between successive frames. The passband transmit signal can be written as follows:

$$s(t) = \Re\left[ e^{j2\pi f_{\text{pt}} t} + \sum_{k=0}^{N_p+N_d-1} x[k] g_T(t - kT) e^{j2\pi f_0 t} \right], \tag{8}$$

where $x[k]$ are phase shift keying (PSK) symbols, $T$ is the modulation symbol duration, and $g_T(t)$ is a pulse-shaping waveform chosen as square root raised cosine (SRRC).

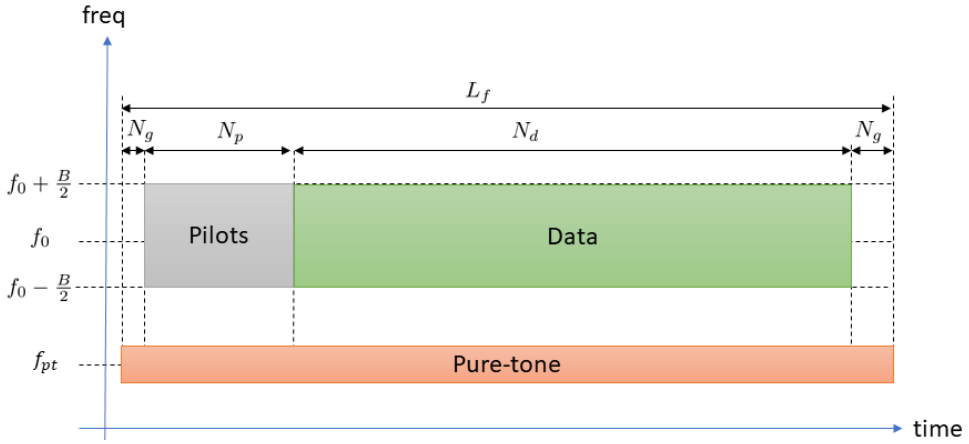


**Figure 3.** Architecture of the communication frame.

On the receiver side, underwater acoustic frames are decoded using the algorithm described in Figure 4. After analog-to-digital conversion, the main signal is base–band translated and match-filtered with an SRRC filter. Frame synchronization is then performed using cross-correlation between matched filtered samples and the pilot sequence. On the other hand, the pure-tone signal is base–band converted and then low pass filtered. Since the motion-induced Doppler shift $f_d$ is linked to relative speed $v_r$ with $f_d = v_r f_{\text{pt}}/c_w$, the low pass filter cutting frequency is set to $f_{\max} = \frac{v_{\max} f_{\text{pt}}}{c_w}$ with $v_{max}$ as the maximum AUV speed and $c_w$ as the sound speed in water. The chosen Doppler estimation algorithm consists of extracting the Doppler shift from the phase derivative of the pure-tone base-band signal $\tilde{r}_{pt}(t)$ by computing the phase angle from two successive samples. As a result, an estimation of the relative speed at sampling time $k$ is formed as follows:

$$\hat{v}_r(kT) = \frac{c_w}{2\pi T f_{pt}} \arg(\tilde{r}_{pt}(kT)\tilde{r}^*_{pt}((k-1)T)). \tag{9}$$

The relative speed estimation is then fed to the SRRC filter in order to match the SRRC response to the Doppler shift effect and to the Doppler compensation stage. In fact, the motion-induced Doppler shift is usually removed from the received useful base-band signal $\tilde{r}(t)$ via resampling and phase compensation [6]:

$$y[k] = \tilde{r}(\hat{t}_k)e^{-j\hat{\phi}_k}, \tag{10}$$

where $\hat{t}_k$ and $\hat{\phi}_k$ are updated dynamically from the instantaneous relative velocity estimation:

$$\begin{cases} \hat{t}_k = \hat{t}_{k-1} + T(1 - \frac{\hat{v}_r(kT)}{c_w}) \\ \hat{\phi}_k = \hat{\phi}_{k-1} + 2\pi f_0 T \frac{\hat{v}_r(kT)}{c_w} \end{cases}. \tag{11}$$

Data decoding is finally performed using the received signal $y[k]$ by advanced equalization processing and channel decoding. In our case, we consider a turbo-equalizer with residual phase compensation as described in [5].

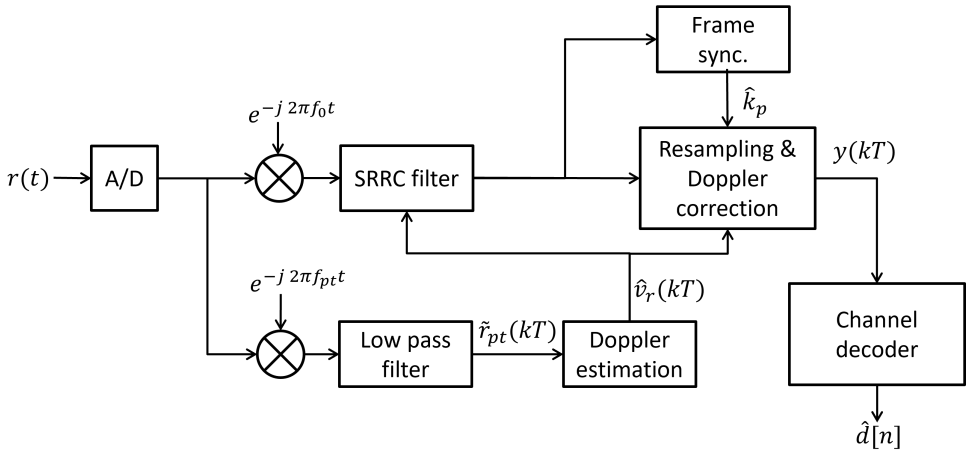


**Figure 4.** Architecture of the communication decoder.

### *3.5. Measurements*

#### 3.5.1. Distance Estimation

The distance estimation $\hat{d}$ is provided by using the frame synchronization process described in Figure 4. By assuming perfect clock synchronization between the beacon and AUV, if a UWA frame is sent at time 0, we can estimate the distance with the TOF of the acoustic signal as follows:

$$\hat{d} = \frac{\hat{t}_0 - N_g T}{c_w}, \tag{12}$$

where $\hat{t}_0$ denotes the estimated time of arrival of the first pilot symbol of the UWA frame. For simplification, this approach is considered in this paper. However, in reality, achieving perfect synchronization between the transmitter and receiver clocks is challenging. One potential solution is to use the pulse per second (PPS) signal from a surface buoy GNSS to aid synchronization for the AUV. The AUV would reproduce this PPS synthetically. But, it drifts over time and is not a long-term solution. This is, for instance, suitable for a micro-AUV. It is also possible to use an atomic clock, but it is not suitable for a micro-AUV because of its size and cost.

Another option is to use bidirectional communication. Using time of emission and communication transit time, it is possible to compute distance estimation. No synchronization between the clocks of the transmitter and receiver is needed. Precise time computation is made through stable electronics. Multiple acoustic sources are commonly used to get the most precise estimation possible. To remove the need for precise emission time knowledge, TDOA is another popular ranging technique. This method only requires the time signal that was received and the speed that the signal travels. Once the signal is received, the difference in arrival time with the last communication is used to calculate the difference in distances.

No matter which technique is used, at least three beacons are necessary to carry out a triangulation and, hence, estimate the position of the AUV. However, in this paper, time of arrival (TOA) and TDOA could be chosen for our unique beacon solution as we only need to know the distance between the beacon and the AUV.

#### 3.5.2. Speed Estimation

Obtaining the projected speed from $\hat{v}_r$ requires two angles, $\omega_b$ and $\psi$, as illustrated in Figure 2, and this is expressed as follows:

$$v_r = v \cdot \cos(\omega_b - \psi). \tag{13}$$

The bearing angle $\omega_b$ is defined as follows:

$$\omega_b = \arctan 2\left(\frac{y - y_{\text{ref}}}{x - x_{\text{ref}}}\right) + \pi. \tag{14}$$

As a result, an estimation of the AUV speed can be formed as follows:

$$\hat{v} = \frac{\hat{v}_r}{\cos\left(\arctan 2(\hat{y} - y_{\text{ref}}, \hat{x} - x_{\text{ref}}) - \hat{\psi}\right)}. \tag{15}$$

If the relative speed estimation $\hat{v}_r$ is provided by the Doppler shift estimation and the heading angle $\hat{\psi}$ comes from the AHRS, Equation (15) requires the knowledge of the AUV position $(\hat{x}, \hat{y})$, which is provided by the prediction state $\mathbf{z}_k$ of the Kalman filter.

#### 3.5.3. Proprioceptive Sensors

Estimates of the heading angle of the drone (yaw angle), labelled $\hat{\psi}$, can be measured either by a low-cost AHRS, which delivers a heading directly (e.g. MTI-630, Xsens, Enschede, Netherlands or ELLIPSE series, SBG systems, Carrières-sur-Seine, France), or by an IMU, which delivers the accelerations, gyroscope (angular rates), and magnetic fields on the $x, y$ and $z$ axes. Magnetic fields are, respectively, $H_x, H_y$ and $H_z$. The magnetic heading is then calculated according to the following method for a 2D plane :

$$\begin{aligned}
&\hat{\psi}(y > 0) = 90 - \arctan(H_x/H_y) \cdot 180/\pi, \\
&\hat{\psi}(y < 0) = 270 - \arctan(H_x/H_y) \cdot 180/\pi, \\
&\hat{\psi}(y = 0, x < 0) = 180, \\
&\hat{\psi}(y = 0, x > 0) = 0.
\end{aligned} \tag{16}$$

The magnetic heading is, however, subject to strong errors from the environment. It is then usual to fuse it to an EKF with acceleration and a gyroscope labelled $\hat{\Omega}$ and $\hat{a}$. The usual sensor noise for a low-cost sensor in static is given for $b_\theta \in [0.1; 1]°$. In dynamics, MEMS inertial unit noises are kept below $b_\theta = 2°$ but drift over time with a bias instability around 5°/h.

#### 3.5.4. Equations

The measurement equation is defined as follows:

$$\begin{cases} \mathbf{y}_k = g(\mathbf{z}_k) + \mathbf{v_k} & \text{if no UWA communication} \\ \mathbf{y}_k^{\text{com}} = g^{\text{com}}(\mathbf{z}_k) + \mathbf{v}_k^{\text{com}} & \text{else} \end{cases}, \tag{17}$$

where $\mathbf{y}_k^{\text{com}}$ is the observation vector, $g^{\text{com}}(.)$ is the observation function when a UWA communication frame is received and then decoded, and $\mathbf{y}_k$ and $g(.)$ are observed when the algorithm is updated in dead-reckoning mode. Observation vectors are defined as follows:

$$\mathbf{y}_k^{\text{com}} = \begin{pmatrix} \hat{d} \\ \hat{v}_r \\ \hat{\psi} \\ \hat{\Omega} \\ \hat{a} \end{pmatrix} \quad \mathbf{y_k} = \begin{pmatrix} \hat{\psi} \\ \hat{\Omega} \\ \hat{a} \end{pmatrix}. \tag{18}$$

The distance between the drone and the reference point can be computed as a function of the drone position:

$$d = \sqrt{(x - x_{\text{ref}})^2 + (y - y_{\text{ref}})^2}. \tag{19}$$

By combining (15), (18), and (19), we obtain the following observation functions:

$$g^{\text{com}}(\mathbf{z}) = \begin{pmatrix} \sqrt{(x - x_{\text{ref}})^2 + (y - y_{\text{ref}})^2} & -v\cos\left(\arctan 2(y - y_{\text{ref}}, x - x_{\text{ref}}) - \psi\right) & \psi & \Omega & a \end{pmatrix}^T$$
$$g(\mathbf{z}) = \begin{pmatrix} \psi & \Omega & a \end{pmatrix}^T \tag{20}$$

### 3.6. Estimator Filter

In the proposed positioning system, we consider the EKF estimator [24,25] described in Algorithm 1. The filter takes as input the state vector and the estimator covariance matrix at sampling step $k-1$, i.e., $\mathbf{z}_{k-1}$ and $\mathbf{P}_{k-1}$, input command vector $\mathbf{u}_k$, and measurement vector $\mathbf{y}_k$. The estimator produces state vector $\hat{\mathbf{z}}_k$ and an updated covariance matrix $\mathbf{P}_{k-1}$. The algorithm requires the state transition matrix $\mathbf{F}$, which is computed as follows.

**Algorithm 1:** Extended Kalman Filter

**Data:** $\mathbf{z}_{k-1}$, $\mathbf{P}_{k-1}$, $\mathbf{u}_k$, $\mathbf{u}_k$
**Result:** $\hat{\mathbf{z}}_k$, $\mathbf{P}_k$
$\mathbf{F} = \nabla_f$;
$\mathbf{H} = \nabla_h$;
$\hat{\mathbf{z}}_k^- = f(\mathbf{z}_{k-1}, \mathbf{u}_k)$;
$\mathbf{P}_k^- = \mathbf{F}\mathbf{P}_{k-1}\mathbf{F}^T + \mathbf{Q}$;
$\mathbf{K}_k = \mathbf{P}_k^-\mathbf{H}^T(\mathbf{H}\mathbf{P}_k^-\mathbf{H}^T + \mathbf{R})^{-1}$;
$\mathbf{y} = (\mathbf{y}_k - h(\hat{\mathbf{x}}_k^-))$;
$\hat{\mathbf{z}}_k = \hat{\mathbf{z}}_k^- + \mathbf{y}\mathbf{K}_k$;
$\mathbf{P}_k = \mathbf{P}_k^- - \mathbf{K}_k\mathbf{H}\mathbf{P}_k^-$.

$$\mathbf{F} = \frac{\partial f}{\partial \mathbf{z}} = \begin{pmatrix} 1 & 0 & -v\cdot\Delta_t\cdot\sin(\psi) & \Delta_t\cdot\cos(\psi) & 0 & 0 \\ 0 & 1 & v\cdot\Delta_t\cdot\cos(\psi) & \Delta_t\cdot\sin(\psi) & 0 & 0 \\ 0 & 0 & 1 & 0 & \Delta_t & 0 \\ 0 & 0 & 0 & 1 & 0 & \Delta_t \\ 0 & 0 & 0 & 0 & 1 & 0 \\ 0 & 0 & 0 & 0 & 0 & 1 \end{pmatrix}, \tag{21}$$

The algorithm also requires the so called observation matrix, which is computed as follows when an UWA communication frame is available:

$$\mathbf{H} = \frac{\partial g_{\text{com}}}{\partial \mathbf{z}} = \begin{pmatrix} 0 & 0 & 1 & 0 & 0 & 0 \\ 0 & 0 & 0 & 0 & 1 & 0 \\ 0 & 0 & 0 & 0 & 0 & 1 \\ A\cdot(x - x_{\text{ref}}) & A\cdot(y - y_{\text{ref}}) & 0 & 0 & 0 & 0 \\ -B\cdot(y - y_{\text{ref}}) & B\cdot(x - x_{\text{ref}}) & -v\cdot\sin(C) & -\cos(C) & 0 & 0 \end{pmatrix}, \tag{22}$$

with

$$A = \frac{1}{\sqrt{(x - x_{\text{ref}})^2 + (y - y_{\text{ref}})^2}}$$
$$B = \frac{v\cdot\sin\left(\arctan 2(y - y_{\text{ref}}, x - x_{\text{ref}}) - \psi\right)}{(x - x_{\text{ref}})^2 + (y - y_{\text{ref}})^2}. \tag{23}$$
$$C = \arctan(y - y_{\text{ref}}, x - x_{\text{ref}}) - \psi$$

In the case of a lack of an UWA communication frame, the observation matrix becomes the following:

$$\mathbf{H} = \frac{\partial g}{\partial \mathbf{z}} = \begin{pmatrix} 0 & 0 & 1 & 0 & 0 & 0 \\ 0 & 0 & 0 & 0 & 1 & 0 \\ 0 & 0 & 0 & 0 & 0 & 1 \end{pmatrix}. \tag{24}$$

Finally, the algorithm requires the covariance matrix of the process noise noted as **Q** and the covariance matrix of measurement noise labelled **R**.

## 4. Results

### 4.1. Simulation

In this section, the performance of the positioning system is studied using simulation. The global architecture of the simulation system is depicted in Figure 5, which includes two main parts exchanging data in an iterative manner: the positioning algorithm (see Figure 1) and the simulation algorithm computing AUV trajectory, generating noises and collecting results. The simulation script is implemented in MATLAB™ 2024 software, and the algorithm is based on the Monte-Carlo method, i.e., each noise datum is random, and the simulation is performed $N_{\text{runs}}$ times in order to average the results.

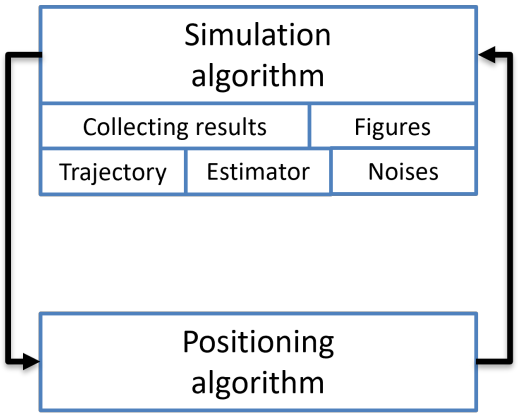


**Figure 5.** Global architecture of the simulation script.

#### 4.1.1. Parameters

The main simulation parameters are summarized in Table 2. The simulated trajectory is a boustrophedon with a traveled distance of 1567 m during around 26 min, representing an average speed of 1 m/s. The algorithm is updated every $\Delta t = 0.25$ s, which is aligned with a frequency update of 4 Hz. The area of the mission is 100 m per 250 m, and the reference beacon is located in the center of this area.

**Table 2.** Simulation parameters.

| Parameters | Description | Value |
|---|---|---|
| $T_{\text{mission}}$ | Mission duration | 1550 s |
| $\Delta t$ | Algorithm time step | 250 ms |
| $T_{\text{com}}$ | UWA communication period | $[3, 20]$ s |
| $N_{\text{runs}}$ | Number of simulation runs | 300 |
| $\begin{pmatrix} x_{\text{ref}} & y_{\text{ref}} \end{pmatrix}^T$ | Beacon position | $\begin{pmatrix} 50 & 100 \end{pmatrix}^T$ |
| $v$ | drone velocity | $[-3, -1] \cup [1, 3]$ m/s |

To obtain accurate results, we conduct $N_{\text{runs}} = 300$ iterations by generating new noise samples for each parameters at each iteration where one iteration gives the following:

- Mean positioning error;
- Variance of the positioning error;
- Root mean square error and positioning error curves;
- Noises for each measurement;
- Bearing angle estimation errors.

At the end of $N_{\text{runs}}$ iterations, each of the values is averaged. The average of the mean positioning error is used to compute outlier results. The outliers are detected if the number is greater than $q_3 + 1.5 \times (q_3 - q_1)$ or less than $q_3 - 1.5 \times (q_3 - q_1)$. These outlier results

are not considered, as it is assumed that the algorithm has diverged or is too far from the true position. For the remainder of this article, we will note the number of simulations that diverged. In the simulation script, the UWA communication process, as described in Section 3.4, is not simulated: estimated range and speed values are only emulated by adding noise representative of estimation errors. Noises from the measurements are shown in three box plots in Figure 6. White Gaussian noises centered around 0 from the IMU (acceleration and angular velocity) are also added, with values contained in $\pm 0.1$ m/s$^2$ and $\pm 0.1$ s$^{-1}$. For the EKF estimator, matrices $\mathbf{R}$ and $\mathbf{Q}$ are defined as follows:

$$\begin{aligned} \mathbf{Q} &= \mathrm{diag}(\Delta_t^8, \cdots, \Delta_t^8) = \mathrm{diag}(0.25^8, \cdots, 0.25^8) \\ \mathbf{R} &= \mathrm{diag}(1 \;\; 0.005 \;\; 0.005 \;\; 12 \;\; 0.2) \end{aligned}, \tag{25}$$

with $\mathbf{Q} \in \mathbb{R}^{6\times 6}$ and $\mathbf{R} \in \mathbb{R}^{5\times 5}$. These covariance matrices are fixed during all simulations.

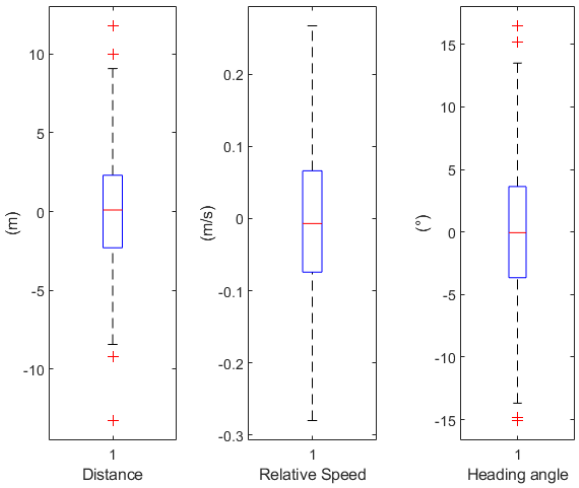


**Figure 6.** Noise statistics added for each mesurements. The central mark indicates the median, and the bottom and top edges of the box indicate the 25th and 75th percentiles, respectively. The outliers are plotted individually using a red cross marker symbol.

#### 4.1.2. Simulation Results

A two-dimensional top-view of the mission is depicted in Figure 7, and the associated statistical results are carried out in Figure 8. To keep the top view as clear as possible, only the four lowest communication periods are exploited. The acoustic beacon, at the same depth of the AUV for 2D simplification, is represented by a blue star marker.

Results are displayed in their entirety in Table 3. Numbers displayed in parenthesis are the number of outliers in the $N_{\text{runs}}$ iterations, whereas %etd (error over traveled distance) denotes the positioning error in percentage of the traveled distance. Whatever the value of $T_{\text{com}}$ is, any divergence of the algorithm is observed; however, as $T_{\text{com}}$ increases, both positioning error and its variance increases. This phenomenon is easily explained by the fact that between two UWA communications, the positioning algorithm works only in dead-reckoning navigation, which results in higher drift errors.

The Boustrophedon-type trajectory is one of the most commonly used trajectories in the AUV and micro-AUV fields, among other trajectories such as pipeline tracking or depth saw-tooth. The objective of a Boustrophedon trajectory is to collect bathymetry and side-scan sonar data. The overlap of scan images has not been taken into account here. Therefore, the positioning results must be linked to the position of the acquired data. Traditional side-scan sonar embedded on ROVs or micro-AUVs has a maximum beam of around 50 m. Results shown in Figure 8 highlight the maximum positioning error at around 18 m after 1500 s of navigation. Furthermore, the peak of these errors occurs during turns (curvilinear sections) where scan and bathymetry data are not necessarily required.

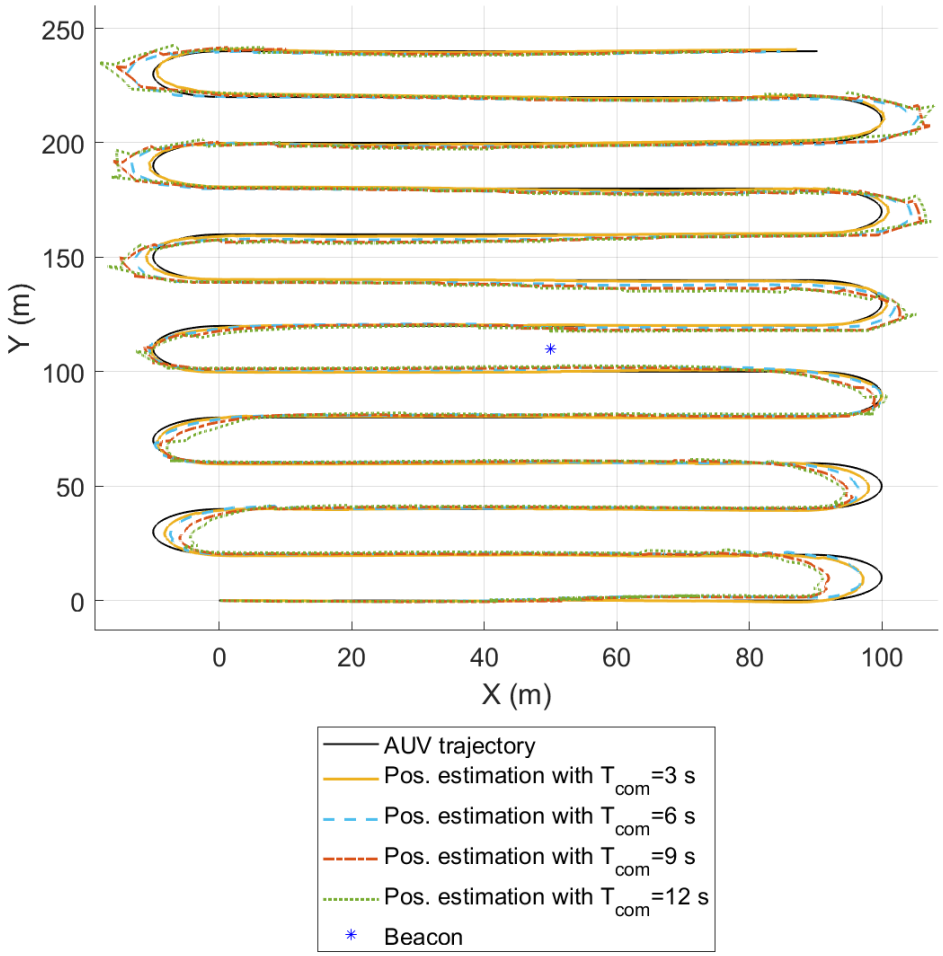


**Figure 7.** Two-dimensional top view of the averaged positioning estimation in comparison to the actual AUV position in black.

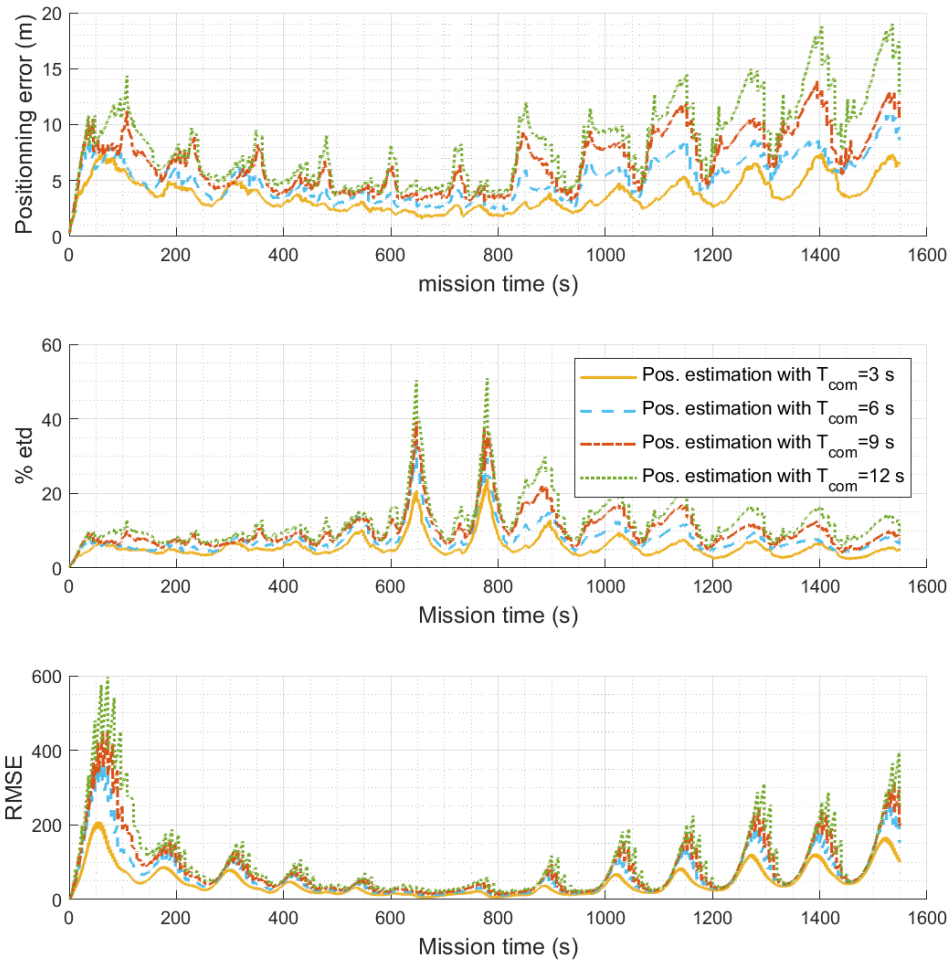


**Figure 8.** Statistical performance results of the simulated positioning system as a function of mission time and the UWA communication period $T_{com}$. **Up**: averaged positioning error (% etd), **middle**: error as a percentage of the traveled distance, and **down**: root mean square error (RMSE).

The lack of linear speed measured by the system (which could be measured through a DVL) induces growing errors during curvilinear sections of the trajectory. This phenomenon can also be explained by the absence of the bearing angle estimation of the UWA communication, which causes a delay in the projection of the relative speed of the AUV.

**Table 3.** Algorithm results for 300 simulated missions.

| $T_{com}$ | Mean Positioning Error (Outliers) in m | Variance of the Positioning Error | %etd Max | %etd Mean |
|---|---|---|---|---|
| 3 s | 3.6054 (1) | 1.7549 | 0.5268 | 0.2281 |
| 6 s | 5.0440 (5) | 3.2143 | 0.5850 | 0.3152 |
| 9 s | 6.4518 (1) | 6.2173 | 0.7662 | 0.4032 |
| 12 s | 8.0853 (6) | 12.7455 | 1.0938 | 0.5053 |
| 15 s | 9.5457 (6) | 18.3823 | 1.3950 | 0.5966 |
| 20 s | 12.1322 (6) | 33.9161 | 1.7825 | 0.7583 |

A comparison between the proposed algorithm and the well-known ROSB technique [10] is provided in Table 4. We can note that the ROSB method is both less accurate and less precise than the proposed method. As $T_{com}$ increases, the difference between the two methods is reduced; however, the number of outliers with the ROSB method increases more and more often.

**Table 4.** Comparison between proposed method and state-of-the-art method, i.e., the ROSB method.

| $T_{\text{com}}$ | Mean Positioning Error (Outliers) in m with Proposed Method | Mean Positioning Error (Outliers) in m with ROSB |
|---|---|---|
| 3 s | 3.6054 (1) | 4.5870 (4) |
| 6 s | 5.0440 (5) | 6.2255 (6) |
| 9 s | 6.4518 (1) | 7.7197 (5) |
| 12 s | 8.0853 (6) | 9.2462 (15) |
| 15 s | 9.5457 (6) | 10.6684 (10) |
| 20 s | 12.1322 (6) | 12.9695 (29) |

The results of these simulations show that for bathymetric or scan data collection, where the position of the data is a critical value, a low-cost positioning system communicating in real time simultaneously with a beacon is effective. In the case of analysis of a large underwater zone, where the accuracy of the data position is important, it is perfectly feasible to make surface ascents to recover the GPS before diving again to continue the mission.

### *4.2. Experiments*

#### 4.2.1. Description

The experiment took place in the Bay of Brest between the 5 and 6 of July 2022. Since the positioning is post-processed, everything was set up so that measurements were data-logged and synchronized using PPS. While moving with a rigid-hull inflatable boat with one hydrophone submerged, data from two GNSS signals (one from the boat and one from the beacon), the hydrophone signal, and measurements from an IMU were recorded. Sound speed was measured hourly using a sound velocity probe (SVP) instrument. The measured sound speed remained constant between 1512 and 1513 m/s over the two days. For simplicity, in the following, we set $c_w$ in the positioning algorithm as an average value during the 2 days of the experiment. In practice, the algorithm should use the instantaneous value of $c_w$ provided by the SVP. The water depth was between 3 and 5 m and the boat speed was between 1 and 5 knots. Other parameters are detailed in Table 5.

From the experiment session, four trajectories were selected in this paper. Due to operational reasons, it was not possible to reproduce exactly the Boustrophedon trajectory detailed in the simulation section. Trajectory #1 is a 10 min long, complex route with many U-turns, but it is close to the beacon. #2 is a 5 min simple and close route. #3 is a 10 min long survey path going further and further away from the beacon. #4 is a 450 m away simple path for 3 min and 20 s. Figure 9 represents the GNSS positioning values of the first trajectory. Acoustic data are processed as described in Section 3.5 in order to estimate both distance $\hat{d}$ and $\hat{v}$, and then estimates are fed to the position algorithm. All the processing scripts are implemented in MATLAB™.

**Table 5.** Experimental parameters.

| Parameters | Description | Value |
|---|---|---|
| $\Delta t$ | Algorithm time step | 1 s |
| $T_{\text{com}}$ | UWA communication period | 3 s |
| $\begin{pmatrix} x_{\text{ref}} & y_{\text{ref}} \end{pmatrix}^T$ | Beacon position | $(48.38243 \text{ lat.}, -4.407295 \text{ long.})^T$ |
| $T_F$ | UWA frame duration | 300 ms |
| $f_{\text{pt}}$ | Pure-tone signal frequency | 20 kHz |
| $f_0$ | Data signal center frequency | 28 kHz |
| $1/T$ | Modulation speed | 6.4 kHz |
| $B$ | Signal bandwidth | 8.96 kHz |
| $f_s$ | Sampling frequency | 96.153 kHz |


**Figure 9.** Map of trajectory #1 made by the boat.

### 4.2.2. Experimental Results

Figures 10 and 11 show the four trajectories chosen for this paper. The blue dashed line represents the ROSB state-of-art positioning estimation, whereas the red dotted line represents the positioning algorithm of this article. Every route starts at $(0, 0)$, and the known position of the buoy is represented as a red star. The real position is the GNSS measurement.

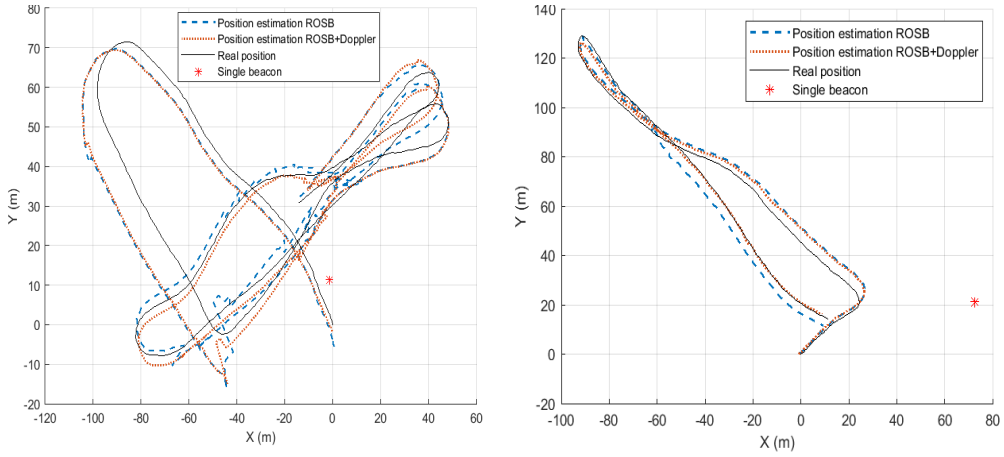


**Figure 10.** Trajectory #1 (**left** ), trajectory #2 (**right**).

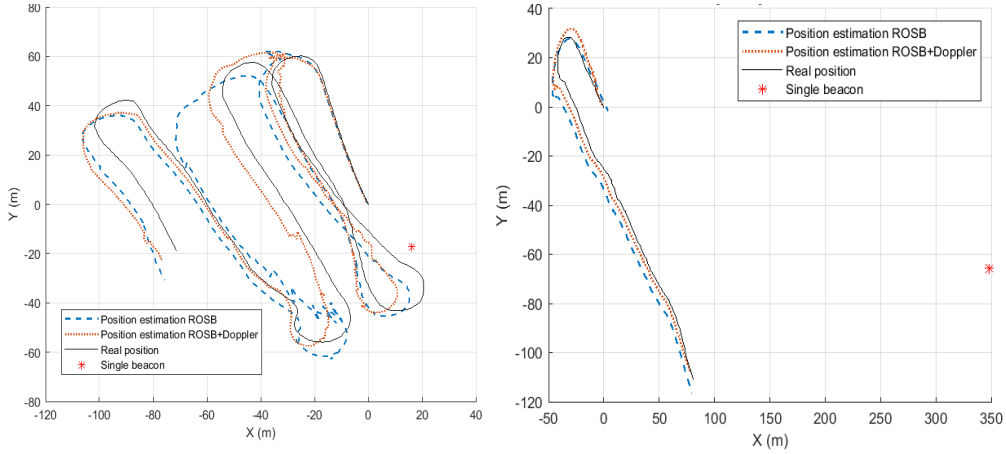


**Figure 11.** Trajectory #3 (**left**), trajectory #4 (**right**).

Table 6 exhibits the mean positioning error for the 4 studied trajectories and a comparison with the state-of-the-art method, i.e., ROSB. Each one of the shown trajectories has a mean positioning error, compared to the GNSS, below 6 m. This is an affirmation that can be extended to all sessions of experimentation regardless of the distance or the complexity of the followed route. However, we can observe that a simpler path is obviously easier to estimate (such as #2) and better closer than further (#2 is better than #4). In all cases and in a similar manner to simulation, the proposed method outperforms the ROSB, demonstrating the interest in estimating the AUV speed through Doppler estimation.

Trajectories #1 and #3 highlight the fact that estimating the relative speed of the AUV using the Doppler of the acoustic communication improves positioning over time compared to the ROSB solution, especially when the drift on heading is important. There are two striking examples in the trajectories cited above. For the first trajectory, around $x = -45$ and $y = -5$, we observe a shift linked to the acoustic communication. In the case of the ROSB, the realignment is too far and degrades positioning accuracy, whereas, in the case of the system proposed in this article, the realignment is correct, allowing the straight line that follows to be positioned accurately. This is important for scan recording. For trajectory #3, the authors would like to draw the reader's attention to the line located after the turn at $x = -50$ and $y = 55$. Of all the trajectories, this is the area where the difference between ROSB and the proposed system is the largest. This can be explained by the start of the turn, where the trajectory estimated by ROSB does not take speed into account and relies on its heading, which leads to errors throughout the rest of the trajectory. The acoustic range observation does not seem to correct this initial error. Unlike a USBL, which provides latitude and longitude measurements, the range information alone does not allow the AUV to be located precisely in the area. In contrast, the trajectory estimated by the proposed system is much better. It is even possible to visually observe the acoustic corrections, although this is still insufficient compared with a USBL/DVL positioning system. Finally, one can notice that, on trajectory #4, during the turn, the ROSB system performs better than the ROSB+Doppler proposed solution. Since the estimated heading at this moment is correct, the addition of the relative speed by Doppler estimation without the bearing angle of the UWA communication degrades the positioning compared with the simpler system. However, the algorithm does not diverge and still estimates the correct position at the end of the turn. This is in line with the simulations carried out with varying degrees of heading error during boustrophedon scan trajectories. At a certain distance from the beacon, the estimated position in turns exceeds the actual position but is correctly aligned in straights.

Figure 12 exhibits the positioning error and RMSE over time for each trajectory, which is the image of the confidence of the EKF estimation. We can see that after 10 min of localization, the error does not grow; thus, the algorithm does not diverge. The error mainly increases during turns for a few reasons:

- The sea current implies a boat drift, which impacts the heading angle, bearing angle and then relative speed $v_r$. In fact, due to (13), we estimate only the forward speed and not the transverse speed.
- The bearing angle is not measured or estimated through UWA but through EKF linearity.
- Between each communication, the EKF only measures the heading angle $\psi$.

Table 7 provides results in the form of percentage error on traveled distance that can be compared with values obtained in simulation (see Table 3). For the first trajectories, the results are very close to the values provided in Table 3. The results of the 4-th trajectory can be explained by the low distance traveled in 200 s; in fact, the boat speed was lower than other trajectories. Moreover, this trajectory has the highest range between beacon and boat, although a less complex y trajectory than other ones. Nevertheless, the proposed method still outperforms ROSB for this trajectory.

Finally, Table 8 provides the mean positioning error as a function of $T_{\text{com}}$. As shown in the simulation, the positioning increases gradually as $T_{\text{com}}$ increases. One can note that for trajectory #1, a divergence of the algorithm is observed for $T_{\text{com}} = 15$ s.

**Table 6.** Experimental results and comparison with state-of-the-art methods.

| Trajectory | Mean Positioning Error in m with Proposed Method | Mean Positioning Error in m with ROSB Method |
|---|---|---|
| #1 ($t_{max}$ = 600 s) | 4.6225 m | 5.4287 m |
| #2 ($t_{max}$ = 300 s) | 2.1537 m | 2.9931 m |
| #3 ($t_{max}$ = 600 s) | 5.0740 m | 8.6719 m |
| #4 ($t_{max}$ = 200 s) | 4.2069 m | 6.2746 m |

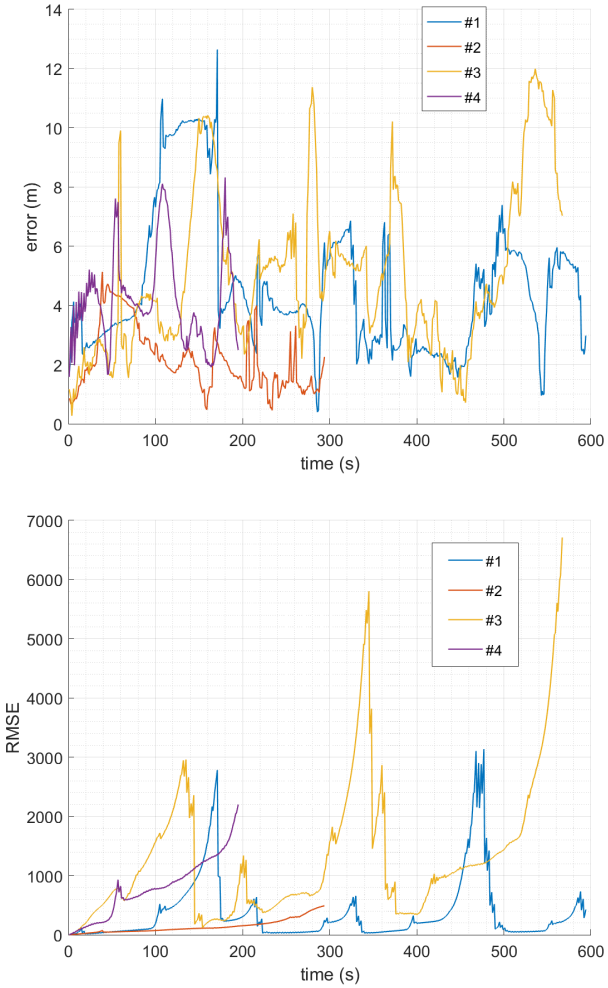


**Figure 12.** Experimental performance of positioning system for the 4-th selected trajectory as function of mission time. **Up**: averaged positioning error, and **down**: error dispersion (RMSE).

**Table 7.** Experimental results in the form of a positioning error as a percentage of the traveled distance for the 4 studied trajectories.

| Trajectory | Traveled Distance in m | %etd Max | %etd Mean |
|---|---|---|---|
| #1 ($t_{max}$ = 600 s) | 698.4989 | 1.7179 | 0.6617 |
| #2 ($t_{max}$ = 300 s) | 353.3752 | 1.4149 | 0.6094 |
| #3 ($t_{max}$ = 600 s) | 681.5850 | 1.7606 | 0.7444 |
| #4 ($t_{max}$ = 200 s) | 190.5176 | 4.1990 | 2.2081 |

**Table 8.** Experimental results of the 4 studied trajectories as function $T_{com}$. The DIV label refers to a divergence of the algorithm.

| $T_{com}$ | Mean Positioning Error for #1 in m | Mean Positioning Error for #2 in m | Mean Positioning Error for #3 in m | Mean Positioning Error for #4 in m |
|---|---|---|---|---|
| 3 s | 4.6225 | 2.1537 | 5.0740 | 4.2069 |
| 6 s | 5.0982 | 3.3472 | 7.1929 | 4.4613 |
| 9 s | 5.6782 | 3.3813 | 7.4395 | 5.0431 |
| 12 s | 6.0585 | 3.4354 | 8.4071 | 5.6932 |
| 15 s | DIV | 2.5071 | 8.2798 | 5.3535 |
| 18 s | 13.71 | 4.4618 | 9.3593 | 7.5195 |

## 5. Conclusions

The objective of this paper was to describe an innovative localization approach using cost-effective sensors for AUV navigation. In the proposed method, the positioning algorithm relies only on an IMU, a pressure sensor and a UWA communication modem, also used to exchange data between the AUV and the surface. By decoding a UWA frame, the AUV can determine, on the one hand, the TOF of the acoustic link (and, thus, the range) via the frame synchronization algorithm and, on the other hand, its relative speed with respect to the beacon owing to the Doppler shift estimation required for UWA channel equalization.

In comparison to the traditional method of beacon range localization, i.e., ROSB, we performed both simulations and conducted experiments to analyze the performance of the proposed approach in depth. Via simulation over a boustrophedon trajectory and using noise representing error measurements, we show that the proposed method outperforms the ROSB method with lower mean positioning error and fewer outliers. The Boustrophedon type of trajectory is one of the most commonly used trajectories in the field of AUVs, along with others such as depth saw-tooth and pipeline tracking. In both simulation and experimentation, the proposed system approaches the planned mission with errors maintained below 20 m. Because the sensors used are cost-effective and low energy (which is critical for a micro-AUV, where autonomy is limited due to the small size of the battery), the acquired data are positioned satisfactorily. The performance of both algorithms is also closely linked to the time between two communication frames; as this time increases, the positioning error increases gradually. The lack of DVL on both solutions impacts the velocity estimation of the AUV and, thus, implies positioning errors and deviation during turns. It is valuable to note that the main error comes from the bearing angle being unknown rather than the lack of the DVL due to the relative speed estimation from the Doppler shift. Nevertheless, it may be considered that in the context of a sonar scan or bathymetry pattern, positioning accuracy during turns is less critical and may be considered by the mission planning operator. The important point, however, is not to cause the navigation algorithm to diverge. It is possible to overcome this problem by making regular ascent to the surface to obtain a GPS fix, which is a subject for future research and implementation. However, a mission at deep depth (e.g., beyond 200 m) is less prone to regular returns to the surface.

On the other hand, INS, in combination with a USBL as used in the state-of-the-art methods, is allegedly more accurate, even if it is difficult to obtain figures as it differs greatly depending on the hardware used for the system. However, it is also true to say that the proposed solution uses less energy (thanks to fewer hydrophones) and is not affected by the error in computing the bearing angle due to the rotation of the USBL head by the waves but only the estimation error by the filter. Due to the simplification of the acoustic computing compared to the USBL, we can also argue that the positioning and data exchange through the UWA channel is more robust. Adding a pure tone before the UWA communication allows an instant Doppler estimation [20].

In the sea environment, the whole positioning system (including the UWA communication link) was evaluated over several trajectories. Experimental results confirmed simulation results, and we showed that using Doppler shift estimation improves the local-

ization estimation of the AUV by increasing overall accuracy compared to state-of-the-art ROSB. The accuracy of the system is fairly independent from the range, but the low-speed propagation of the sound underwater will reduce the frequency of UWA communications at long range, which then implies an increase in the positioning error. However, in our algorithm, only forward speed in estimated; thus, transverse speed due to current is not estimated. Therefore, the performance of the proposed system will be substantially affected in case of a large current w.r.t. to forward speed of the AUV. Moreover, we assume perfect timing synchronization between the beacon and AUV; a large timing error between beacon and AUV will result in a Doppler-shift effect at the receiving end, yielding to an erroneous speed estimation error. This phenomenon can be mitigated by measuring this clock drift at the beginning of the mission and by compensating it with Doppler-shift estimation.

In addition, we demonstrated that with a very simple architecture, positioning approximation is possible, and then small AUV navigation can be considered using cost-efficient transducers. Having real-time communication between the AUV and the base of operations is a critical issue, whether for real-time data acquisition without waiting for the end of the mission or a return to the surface or for applications where time is critical, such as mine detection or the detection of a vessel in distress. This simple architecture with an acoustic transponder also opens up a whole range of possibilities. It is feasible to communicate with multiple AUVs while repositioning them from a single beacon. This would make it possible to carry out several short missions to cover a large area with small AUVs, reducing problems of autonomy or positioning error over the long term.

Future work will focus on three-dimensional positioning, adding inertial unit measurements, and pressure sensor implementation. In addition, emphasis will be placed on the measurement covariance matrix as it is possible to obtain the matrix variable, depending on the signal-to-noise ratio (SNR) of UWA acoustic channel, for example.

**Author Contributions:** Conceptualization, R.G., P.F. and P.-J.B.; methodology, R.G., B.T. and C.V.; software, R.G.; writing—original draft preparation, R.G. and P.-J.B.;writing—review and editing, P.F., C.V. and B.T. All authors have read and agreed to the published version of the manuscript.

**Funding:** This research received no external funding.

**Informed Consent Statement:** Not applicable.

**Data Availability Statement:** The raw data supporting the conclusions of this article will be made available by the authors on request.

**Conflicts of Interest:** The authors declare no conflicts of interest.

## References

1. Ridao, P.; Carreras, M.; Ribas, D.; Sanz, P.J.; Oliver, G. Intervention AUVs: The Next Challenge. *IFAC Proc. Vol.* **2014**, *47*, 12146–12159. [CrossRef]
2. González-García, J.; Gómez-Espinosa, A.; Cuan-Urquizo, E.; García-Valdovinos, L.G.; Salgado-Jiménez, T.; Cabello, J.A.E. Autonomous Underwater Vehicles: Localization, Navigation, and Communication for Collaborative Missions. *Appl. Sci.* **2020**, *10*, 1256. [CrossRef]
3. Gussen, C.M.G.; Diniz, P.S.R.; Campos, M.L.R.; Martins, W.A.; Costa, F.M.; Gois, J.N. A Survey of Underwater Wireless Communication Technologies. *J. Commun. Inf. Syst.* **2016**, *31*, 242–255. [CrossRef]
4. Stojanovic, M.; Beaujean, P.P.J. Acoustic Communication. In *Springer Handbook of Ocean Engineering*; Dhanak, M.R., Xiros, N.I., Eds.; Springer International Publishing: Cham, Switzerland, 2016; pp. 359–386. [CrossRef]
5. Bouvet, P.; Auffret, Y.; Munck, D.; Pottier, A.; Janvresse, G.; Eustache, Y.; Tessot, P.; Bourdon, R. Experimentation of MIMO underwater acoustic communication in shallow water channel. In Proceedings of the OCEANS 2017—Aberdeen, Aberdeen, UK, 19–22 June 2017; pp. 1–6. [CrossRef]
6. Eggen, T.H.; Baggeroer, A.B.; Preisig, J.C. Communication over Doppler spread channels. Part I: Channel and receiver presentation. *IEEE J. Ocean. Eng.* **2000** *25*, 62–71. [CrossRef]
7. Paull, L.; Saeedi, S.; Seto, M.; Li, H. AUV Navigation and Localization: A Review. *IEEE J. Ocean. Eng.* **2014**, *39*, 131–149. [CrossRef]
8. Thomson, D. Acoustic Positioning Systems—The Hydrographic Society UK. Available online: https://www.yumpu.com/en/document/view/10350341/acoustic-positioning-systems-the-hydrographic-society-uk (accessed on 17 May 2022).

9. Kaushik, A.; Singh, R.; Dayarathna, S.; Senanayake, R.; Di Renzo, M.; Dajer, M.; Ji, H.; Kim, Y.; Sciancalepore, V.; Zappone, A.; et al. Toward Integrated Sensing and Communications for 6G: Key Enabling Technologies, Standardization, and Challenges. *IEEE Commun. Stand. Mag.* **2024**, *8*, 52–59. [CrossRef]
10. Masmitjà Rusiñol, I. Acoustic Underwater Target Tracking Methods Using Autonomous Vehicles. Ph.D. Thesis, Universitat Politècnica de Catalunya, Barcelona, Spain, 2020.
11. Hunt, M.M.; Marquet, W.M.; Moller, D.A.; Peal, K.R.; Smith, W.; Spindel, R.C. *An Acoustic Navigation System*; Woods Hole Oceanographic Institution: Woods Hole, MA, USA, 1974.
12. Yuan, M.; Li, Y.; Li, Y.; Pang, S.; Zhang, J. A fast way of single-beacon localization for AUVs. *Appl. Ocean. Res.* **2022**, *119*, 103037. [CrossRef]
13. Casey, T.; Guimond, B.; Hu, J. Underwater Vehicle Positioning Based on Time of Arrival Measurements from a Single Beacon. In Proceedings of the OCEANS, Vancouver, BC, Canada, 29 September–4 October 2007; pp. 1–8. . ISSN: 0197-7385. [CrossRef]
14. Vickery, K. Acoustic positioning systems. A practical overview of current systems. In Proceedings of the 1998 Workshop on Autonomous Underwater Vehicles (Cat. No.98CH36290), Cambridge, MA, USA, 21 August 1998; pp. 5–17. [CrossRef]
15. LaPointe, C.E.G. Virtual Long Baseline (VLBL) Autonomous Underwater Vehicle Navigation Using a Single Transponder. Mater's Thesis, Massachusetts Institute of Technology, Cambridge, MA, USA, 2006; p. 94.
16. iXblue. RAMSES Sparse-LBL Positioning System Datasheet. Available online: https://www.ixblue.com/wp-content/uploads/2021/12/ramses-lbl-transceiver-datasheet.pdf (accessed on 17 May 2022).
17. Diamant, R.; Wolff, L.M.; Lampe, L. Location Tracking of Ocean-Current-Related Underwater Drifting Nodes Using Doppler Shift Measurements. *IEEE J. Ocean. Eng.* **2014**, *40*, 887–902. [CrossRef]
18. Aubry, C.; Forjonel, P.; Bouvet, P.; Pottier, A.; Auffret, Y. On the use of Doppler-shift estimation for simultaneous underwater acoustic localization and communication. In Proceedings of the OCEANS 2019—Marseille, Marseille, France, 17–20 June 2019; pp. 1–5. [CrossRef]
19. Garin, R.; Vanwynsberghe, C.; Forjonel, P.; Tomasi, B.; Bouvet, P.J. Simultaneous underwater acoustic localization and communication: An experimental study. In Proceedings of the OCEANS 2021: San Diego—Porto, San Diego, CA, USA, 20–23 September 2021; pp. 1–6. [CrossRef]
20. Garin, R.; Bouvet, P.J.; Forjonel, P.; Tomasi, B. Sea experimentation of single beacon simultaneous localization and communication for AUV navigation. In Proceedings of the OCEANS 2023, Limerick, Ireland, 5–8 June 2023.
21. UCNL Website. Available online: https://unavlab.com/en/o-nas/articles/myi-sdelali-samyiy-malenkiy-i-samyiy-deshevyiy-v-mire-gidroakusticheskiy-modem-uwave/ (accessed on 12 October 2024).
22. Waterlinked Website. Available online: https://waterlinked.com/shop/modem-m16-186 (accessed on 12 October 2024).
23. ArduPilot Website. Available online: https://ardupilot.org/ (accessed on 30 August 2024).
24. Julier, S.; Uhlmann, J.; Durrant-Whyte, H. A new approach for filtering nonlinear systems. In Proceedings of the 1995 American Control Conference—ACC'95, Seattle, WA, USA, 21–23 June 1995; Volume 3; pp. 1628–1632. [CrossRef]
25. Julier, S.; Uhlmann, J.; Durrant-Whyte, H. A new method for the nonlinear transformation of means and covariances in filters and estimators. *IEEE Trans. Autom. Control.* **2000**, *45*, 477–482. [CrossRef]